Competitive uptake of dimethylamine and trimethylamine against ammonia on acidic particles in marine atmospheres

Dihui Chen[1], Xiaohong Yao[1,2*], Chak K. Chan[3*], Xiaomeng Tian[3], Yangxi Chu[4], Simon L. Clegg[5], Yanjie Shen[1], Yang Gao[1,2], Huiwang Gao[1,2]

[1]Key Laboratory of Marine Environment and Ecology (MoE), and Frontiers Science Center for Deep Ocean Multispheres and Earth System, Ministry of Education, Ocean University of China, Qingdao, China

[2]Laboratory for Marine Ecology and Environmental Sciences, Qingdao National Laboratory for Marine Science and Technology, Qingdao, China

[3]School of Energy and Environment, City University of Hong Kong, Hong Kong, China.

[4]State Key Laboratory of Environmental Criteria and Risk Assessment, Chinese Research Academy of Environmental Sciences, Beijing, 100012, China

[5]School of Environmental Sciences, University of East Anglia, Norwich NR4 7TJ, UK

[*]correspondence to: Xiaohong Yao (xhyao@ouc.edu.cn), Chak K. Chan (chak.k.chan@cityu.edu.hk)

Abstract

Alkaline gases such as NH_3 and amines play important roles in neutralizing acidic particles in the atmosphere. Here, two common gaseous amines (dimethylamine (DMA) and trimethylamine (TMA)), NH_3, and their corresponding ions in $PM_{2.5}$ were measured semi-continuously using an Ambient Ion Monitor-Ion Chromatography (AIM-IC) system in marine air during a round-trip cruise of approximately 4000 kilometers along the coastline of eastern China. The concentrations of particulate DMA, detected as $DMAH^+$, varied from <4 ng m^{-3} to 100 ng m^{-3} and generally decreased with increasing atmospheric NH_3 concentrations. Combining observations with thermodynamic equilibrium calculations using the Extended Aerosol Inorganics Model (E-AIM) indicated that the competitive uptake of DMA against NH_3 on acidic aerosols generally followed thermodynamic equilibria and appeared sensitive to DMA/NH_3

molar ratios, resulting in molar ratios of $DMAH^+$ to $DMA+DMAH^+$ of 0.31 ± 0.16 (average+/-standard deviation) at atmospheric NH_3 concentrations over 1.8 μg m^{-3} (with a corresponding DMA/NH_3 ratio of $(1.8 \pm 1.0) \times 10^{-3}$), 0.80 ± 0.15 at atmospheric NH_3 concentrations below 0.3 μg m^{-3} (with a corresponding DMA/NH_3 ratio of $(1.3 \pm 0.6) \times 10^{-2}$), and 0.56 ± 0.19 in the remaining cases. Particulate TMA concentrations, detected as $TMAH^+$, ranged from <2 ng m^{-3} to 21 ng m^{-3}, and decreased with increasing concentrations of atmospheric NH_3. However, $TMAH^+$ was depleted concurrently with the formation of NH_4NO_3 under low concentrations of atmospheric NH_3, contradictory to the calculated increase in the equilibrated concentration of $TMAH^+$ by the E-AIM.

TOC ART

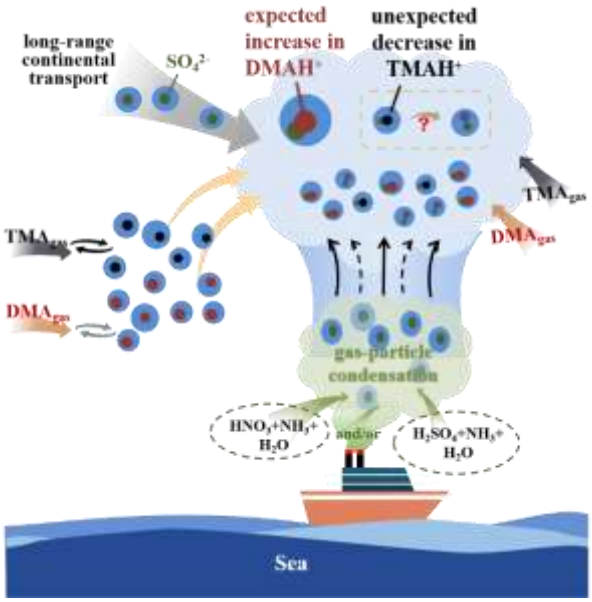

Synopsis

This study reveals the uptake of dimethylamine and trimethylamine against ammonia on acidic particles in ambient air and dispersed combustion plumes.

Keywords: acid-base neutralization, dimethylamine, trimethylamine, ammonia, gas-aerosol partitioning.

1. Introduction

Acid-base reactions are an important pathway in the formation of secondary inorganic and organic particulate matter in the atmosphere.[1–9] Ammonia is the most abundant alkaline gas in the atmosphere;[10,11] its uptake by acidic aerosols, followed by acid-base neutralization reactions, influences air quality, acid rain, and the climate.[12–15] Alkylamines, as derivatives of ammonia, have stronger alkalinity than ammonia and may potentially compete with ammonia to participate in atmospheric acid-base reactions.[1,16–20] For example, dimethylamine (DMA), one of major amines in the atmosphere,[1,2,21] has been recently reported to overwhelm atmospheric ammonia in generating new particles through neutralizing sulfuric acid.[3–7] However, the neutralization of acids by amines such as DMA and trimethylamine (TMA) may be more complicated than by ammonia. For example, completely neutralized $(TMAH)_2SO_4$ in aqueous droplets has been reported to convert to a bisulfate solution, whereas $(DMAH)_2SO_4$ in aqueous droplets equilibrates to $(DMAH_3)H(SO_4)_2$, which is analogous to letovicite .[20,22-23]

The competition between gaseous amines and ammonia to neutralize acidic particles has been investigated through laboratory experiments and simulated in 3-D global and regional models.[18,20,22–28] At ambient temperature (298 K), the dissociation constant (K_b)

of DMA(aq) and TMA(aq) in water is 31 and 4 times of that of NH_3(aq), respectively.[1] (Here, DMA(aq), TMA(aq), and NH_3(aq) refer to their dissolved undissociated states in water, whereas DMA, TMA, and NH_3 refer to their gaseous forms. However, the concentrations of DMA and TMA in ambient air were frequently 2 to 3 orders of magnitude lower than that of NH_3.[2,29–31] Under such large differences in neutralization abilities and ambient concentrations, the competitive uptake of DMA and TMA against NH_3 on acidic particles in ambient air remains poorly understood.

To study this issue, we designed a marine cruise study where both alkaline gases and their particulate counterparts were detected simultaneously. The cruise traveled along a coastline of approximately 4000 kilometers, with varying concentrations of DMA, TMA, and NH_3 because of different marine primary production caused by combinations of factors such as ocean farming, runoff inputs, atmospheric deposition, etc.[32] The vessel was equipped with a URG-9000D Ambient Ion Monitor-Ion chromatography (AIM-IC) system (Thermo-Fisher), used to semi-continuously measure the concentrations of alkaline gases and their particulate counterparts in marine atmospheres. When the instrument was situated downwind of the combustion plumes from the vessel and diluted combustion plumes from other vessels, the competitive uptake of ambient DMA and TMA against NH_3 on the abundant fresh acidic particles in the emissions could thereby be monitored in semi-real time. In other situations, the competitive uptake in clean marine or slightly polluted atmospheres was captured.

2. Experimental

The cruise was conducted aboard the commercial cargo ship, Anqiang 87, along the coastline of the East China Sea, South China Sea, and Yellow Sea, which was approximately 4000 kilometers, from April 20 to May 16, 2018 (Fig 1ab). A suite of instruments was used to measure the gas and particle concentrations in the atmosphere, including an AIM-IC; CO (Thermo Fisher Scientific Model 48i), SO_2 (Thermo Fisher Scientific Model 43i), and NOx (Thermo Fisher Scientific Model 42i) gas analyzers; a Fast Mobility Particle Sizer (FMPS, TSI Model 3091); a CCN counter (CCNC, DMT Model 100); and a Condensation Particle Counter (CPC, TSI Model 3775). A number of off-line samplers were also available to collect air pollutants for chemical analysis. An on-board automatic weather station was used to measure ambient temperature and relative humidity (RH).

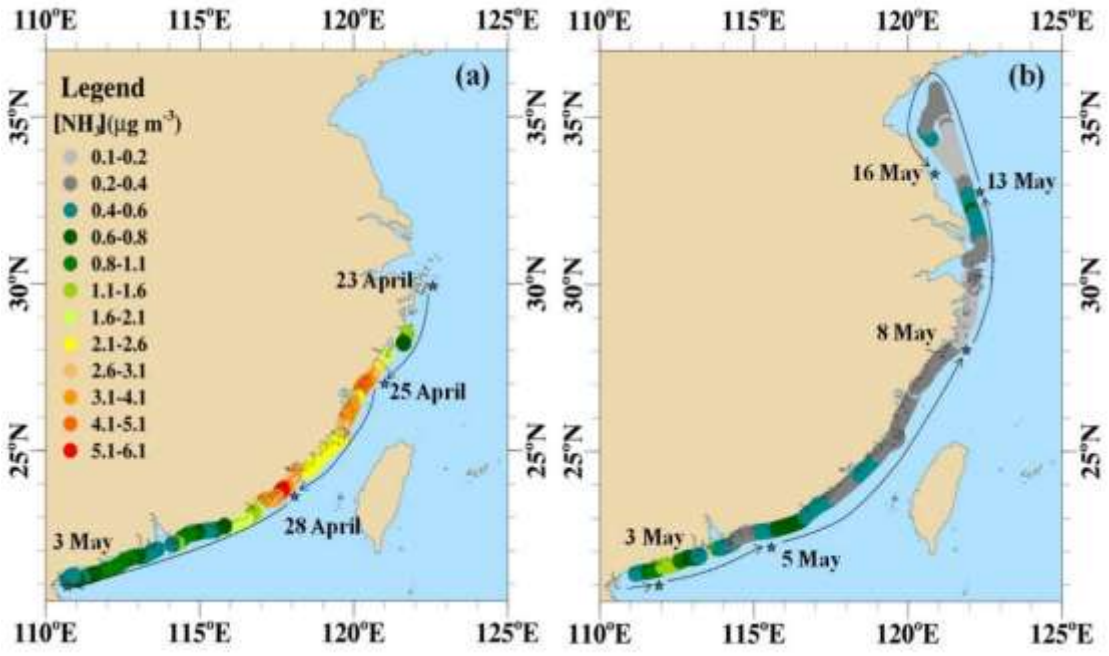

Fig 1. Spatiotemporal variations in mass concentrations of atmospheric NH_3 along the coastline of eastern China. Atmospheric NH_3 along the path of the vessel during (a)

April 23 to May 3 and (b) May 3 to May 16.

The AIM-IC was housed in an air-conditioned container with the inlet approximately 5 m above sea level, whereas all other instruments were housed in another air-conditioned container on the open deck. The AIM-IC was installed with a $PM_{2.5}$ cyclone, which operated at a rate of 3 L min^{-1}, and reported semi-continuous concentrations for chemically reactive gases (NH_3, DMA, TMA, SO_2, HNO_3, etc.) and water-soluble ions in $PM_{2.5}$ at a one-hour time resolution. The ICS-1100 Ion Chromatography of the AIM-IC was equipped with two analytical columns (Ion Pac CS17A (2×250 mm) for cations and Ion Pac AS11-HC (2×250 mm) for anions) and two guard columns (CG17A (2×50 mm) for cations and AG11-HC (2×50 mm) for anions). The detection limits for NH_4^+, $DMAH^+$, and $TMAH^+$ were 0.04, 0.08, and 0.04 μg L^{-1} in injection solution, respectively, corresponding to 2, 4, and 2 ng m^{-3} in the ambient air (more details can be found in Supporting Information). Half of the detection limits were used to represent the concentrations of ions below those limits, which is an approach conventionally adopted in the literature. Helsel, however, reported that the Kaplan–Meier procedure should be used to compute the mean values of data that include nondetects[33]. The comparison between the conventional approach and the Kaplan–Meier procedure were provided in Supporting Information. The uncertainties of ions were determined through multiple injections of standard samples in different concentrations at the beginning, intermediate maintenance and ending of the cruise period. The uncertainty for NH_4^+ was 5% when its measured concentration in the injection solution was above 4 μg L^{-1} (corresponding to 0.2 μg m^{-3} NH_4^+ in ambient air). The uncertainties of $DMAH^+$ and

129 $TMAH^+$ were 41% and 13%, respectively, when their concentrations in the injection
130 solution were above 0.2 μg L^{-1} (corresponding to 10 ng m^{-3} $DMAH^+$ and $TMAH^+$ in
131 ambient air). The uncertainty of $DMAH^+$ decreased to 14% when its concentration was
132 over 50 ng m^{-3} in ambient air. Larger uncertainties were expected for the measured
133 concentrations of $DMAH^+$ and $TMAH^+$ below 10 ng m^{-3} in the ambient air, although
134 they were still detected. More detailed information on AIM-IC analysis can be found in
135 our previous studies.[16-17,34]
136
137 The Extended Aerosol Inorganics Model (E-AIM)
138 (http://www.aim.env.uea.ac.uk/aim/aim.php)[35] was used to calculate the equilibrium
139 concentrations of compounds in gas and particle phases. The measured concentrations
140 in both the gas phase and $PM_{2.5}$, which included NH_3, TMA, DMA, and HNO_3 and their
141 corresponding particulate counterparts, as well as ambient temperature and RH, were
142 used as inputs to calculate the equilibrium concentrations. Na^+ and Cl^- were not
143 included since they were derived mainly from sea-salt aerosols and mostly found in the
144 coarse mode. The E-AIM requires the sum of the equivalent concentrations of the
145 anions in the initial input to equal that of the cations. Thus, either the H^+ or OH^-
146 concentration was used as an additional input to adjust the ionic balance. Nevertheless,
147 the calculated aerosol in-situ pH was less than 4.5 regardless of whether the additional
148 input was H^+ or OH^-. Therefore, the calculated pH value was not sensitive to the
149 additional input. Note that no aerosol organic phase was included in the E-AIM,
150 although it may have existed in the ambient particles.[16,24,36-38]

3 Results and discussion

3.1 Spatiotemporal variations in the concentrations of NH_3, DMA, and TMA

Fig 1ab and Fig 2a show the spatiotemporal variations in the mass concentration of NH_3 ([NH_3]) over the coastline of eastern China. The [NH_3] varied from 0.12 μg m^{-3} to 6.1 μg m^{-3}, with an average (+/- standard deviation) of 1.2±1.3 μg m^{-3} throughout the study. There were two distinct periods in the concentration trend. Period 1 was characterized by higher concentrations of 2.8±1.2 μg m^{-3}, during April 20–30 along the southbound track (Fig 1a; shaded pink in Figure 2). Period 2 was characterized by substantially lower concentrations of 0.43±0.26 μg m^{-3}, during May 1–16; the vessel travelled along the southbound track on May 1–3 and along the northbound track afterwards (Fig 1ab). There were three major SO_2 plumes (shaded grey in Fig 2a) without obvious increases in [NH_3], which were attributed to the emissions of the vessel. Note that vessels on coastal waters in China were not required to use low-sulfur content diesel until 2020; thus, high SO_2 emissions from vessels were common during our study.

Spatiotemporal variations in the mass concentration of DMA ([DMA]) are shown in Fig 2b. The [DMA] was 11±6.5 ng m^{-3}, which was approximately two orders of magnitude smaller than the [NH_3]. The spatiotemporal pattern in the [DMA] was generally consistent with that in [NH_3] during Period 1. However, higher [DMA] values were recorded until May 5 and then decreased (Fig 2b). The [TMA] was lower at approximately 5.4±2.4 ng m^{-3} (Fig 2c). The spatiotemporal pattern in the [TMA] was

distinctly different from those of the [NH_3] and [DMA]. For example, lower [TMA] values were generally observed during Period 1, except a few higher values on April 23–24, when the [TMA] was approximately 9.6±2.4 ng m^{-3}, which was approximately three times larger than the simultaneously measured [DMA] of 2.4±1.3 ng m^{-3}. When Period 1 and May 1–2 of Period 2 were combined for analysis, [TMA] showed the opposite trend to [NH_3], as shown in Fig 2a and 2c. The different concentrations throughout the study may have been caused by differences in marine primary production and complicated emission, transport, and conversion processes.[10,26,28] Additional data, such as ionic concentrations in the sea surface microlayer (from dozens of micrometers to a few centimeters) and bulk surface sea water, are usually needed to explore these causes, but these data were not available in this study.

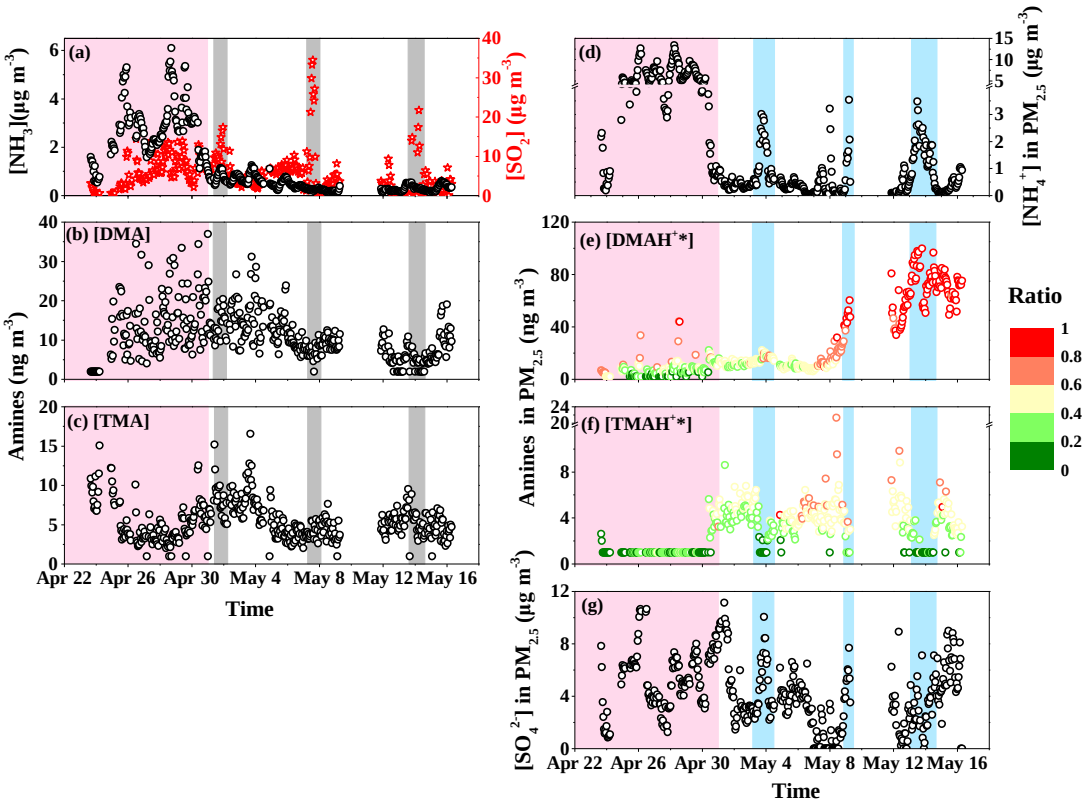

Fig 2. Time series of the gas and particulate ion concentrations, in which Period 1 is highlighted in pink and the remainder is Period 2. (a) NH_3 and SO_2; (b) DMA; (c) TMA; (d) particulate NH_4^+; (e) particulate $DMAH^{+*}$; (f) particulate $TMAH^{+*}$; (g) particulate SO_4^{2-}. The colored bars represent the molar ratios of $DMAH^{+*}$/($DMAH^{+*}$+DMA) in (d) and $TMAH^{+*}$/($TMAH^{+*}$+TMA) in (f). Three SO_2 plumes due to emissions from the vessel are highlighted in gray and three troughs of $TMAH^{+*}$ are highlighted in blue.

3.2 Spatiotemporal variations in the concentrations of NH_4^+, $DMAH^{+*}$, and $TMAH^{+*}$

Fig 2d-f showed the spatiotemporal variations in the mass concentration of three cations in $PM_{2.5}$. The mass concentrations of NH_4^+ ($[NH_4^+]$) varied significantly throughout the study (Fig 2d). For example, Period 1 had high concentrations of 5.4±3.1 μg m^{-3}, but Period 2 had lower concentrations of 0.65±0.71 μg m^{-3}, except for a few spikes that were concurrent with SO_4^{2-} and/or NO_3^- peaks (data in blue shades in Fig 2d, 2g and S1a). During Period 2. these spikes were probably related to particles in the combustion plumes of the vessel and/or other combustion plumes, as indicated by SO_2, HNO_3 or CO (Fig 2a and S1bc). Excluding these spikes, the data during Period 2 reflects either clean or slightly polluted marine atmospheres. Moreover, $[NH_4^+]$ were significantly correlated with $[NO_3^-]$ and $[SO_4^{2-}]$, with an R^2=0.48 and P<0.01.

The particulate $DMAH^+$ measured by AIM-IC may contain both $DMAH^+$ in aerosol aqueous phase and non-dissociated DMA in the aerosol organic phase,[16-17,39-41] however, we could not separate them. Hence, $DMAH^{+*}$ was used instead of $DMAH^+$ in the following analyses. The same is true for $TMAH^{+*}$. NH_4^+ in the aerosol organic phase may have been minor. [41] The $[DMAH^{+*}]$ in $PM_{2.5}$ ranged from <4 ng m^{-3} to 100 ng m^{-3} and generally showed an opposite trend to the corresponding $[NH_4^+]$ in $PM_{2.5}$, except for periods with intense $[NH_4^+]$ spikes during Period 2 (shaded blue in Fig 2d and 2e).

212 The [$DMAH^{+*}$] was low, at 7.4±6.8 ng m^{-3}, during Period 1. It increased slightly to
213 15±9.4 ng m^{-3} during May 2–9, then increased dramatically to 68±15 ng m^{-3} during
214 May 11–16. In the three blue highlighted periods in Figure 2 with [NH_4^+] spikes and
215 [$TMAH^{+*}$] troughs, the [$DMAH^{+*}$] sometimes followed the [NH_4^+] trend, but
216 sometimes it did not. In later analyses, we sub-classified Period 2 into Period 2-A (May
217 1–9) and Period 2-B (May 11–16).
218
219 The [$TMAH^{+*}$] in $PM_{2.5}$ fluctuated from <2 ng m^{-3} to 21 ng m^{-3} and showed a trend
220 opposite that of the [NH_4^+] (Fig 2d and 2f). For example, the [$TMAH^{+*}$] was generally
221 undetectable during Period 1, but prominently and concurrently increased with the
222 dramatic decreases in the [NH_4^+] and [NH_3] on April 30 and May 1. During Period 2,
223 the average [$TMAH^{+}$*] was 3.8±2.0 ng m^{-3}.
224
225 Even in Period 2, with detectable $TMAH^{+*}$, the [$TMAH^{+*}$] in $PM_{2.5}$ was less than the
226 [$DMAH^{+*}$] by several times to over one order of magnitude. Since the [TMA] of
227 5.0±1.5 ng m^{-3} was comparable to the [DMA] of 6.6±3.8 ng m^{-3} during Period 2B, the
228 lower [$TMAH^{+*}$] during that period may have resulted from gas-aerosol
229 partitioning,[26,28] which will be further examined in Section 3.3 and 3.4. Note that either
230 the [$TMAH^{+*}$] lower than the [$DMAH^{+*}$] or the reverse had been observed in marine
231 atmospheric particles collected over different oceanic zones or in different seasons
232 during our previous cruise studies.[16,17,40,41] For example, the [$TMAH^{+*}$] in $PM_{2.5}$ or
233 PM_{10} sometimes varied from hundreds of ng m^{-3} to over 1 μg m^{-3} and thus was

substantially larger than [$DMAH^{+*}$].[40,41]

3.3 Correlations between $DMAH^{+*}$ or $TMAH^{+*}$ and NH_3

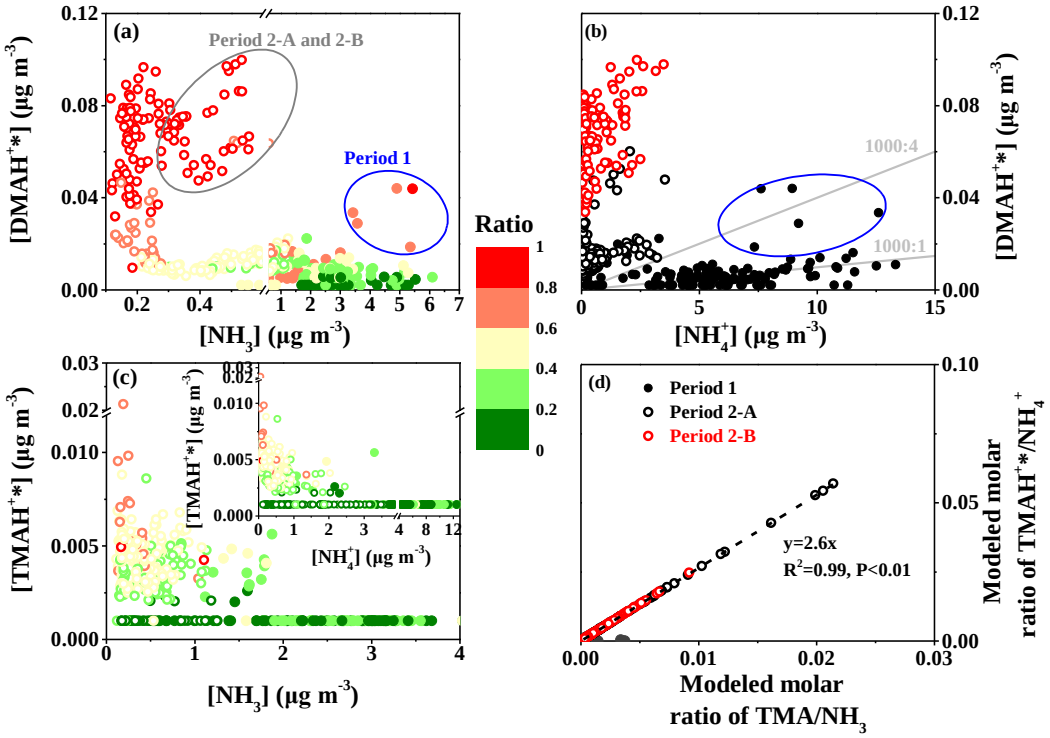

Fig 3. (a) [$DMAH^{+*}$] versus [NH_3]; (b) [$DMAH^{+*}$] versus [NH_4^+]; (c) [$TMAH^{+*}$] versus [NH_3], and [$TMAH^{+*}$] versus [NH_4^+] in the superimposition; (d) modeled $TMAH^{+*}/NH_4^+$ molar ratio versus modeled TMA/NH_3 molar ratio. The colored bar represents the $DMAH^{+*}/(DMAH^{+*}+DMA)$ molar ratio in (a) and the $TMAH^{+*}/(TMAH^{+*}+TMA)$ ratio in (c). Filled and empty markers represent the measurement dates during Period 1 and Period 2, respectively. The definition of the markers in (b) and (d) are identical. The data points circled in blue and in grey represent high concentrations of $DMAH^{+*}$ that occurred with NH_4^+ spikes during Period 1 and Period 2, respectively.

In crystallized ammonium salts or deliquesced droplets, NH_3 may react with aminium salts or their solutions and subsequently release DMA and TMA to the gas phase according to the involved thermodynamic equilibria.[1, 20-21] We analyzed the correlations between the [$DMAH^{+*}$] and [$TMAH^{+*}$] in $PM_{2.5}$ and the [NH_3]. Generally, lower

252 [$DMAH^{+*}$] values and smaller $DMAH^{+*}$/($DMAH^{+*}$+DMA) molar ratios were
253 concurrently observed with higher [NH_3] values (Fig 3a). For example, the [$DMAH^{+*}$]
254 was generally less than 10 ng m^{-3} when [NH_3] was greater than 1.8 μg m^{-3}, with a
255 $DMAH^{+*}$/($DMAH^{+*}$+DMA) molar ratio of approximately 0.31±0.16, which indicated
256 that DMA species in the atmosphere mainly existed as DMA at high NH_3 levels. The
257 reverse was generally true when the [NH_3] was <0.3 μg m^{-3}, in this case the [$DMAH^{+*}$]
258 ranged from 8 ng m^{-3} to 100 ng m^{-3}, with a $DMAH^{+}$*/($DMAH^{+}$*+DMA) ratio of
259 0.80±0.15, indicating that DMA species in the atmosphere mainly existed as $DMAH^{+*}$
260 at low NH_3 levels. The $DMAH^{+}$*/($DMAH^{+}$*+DMA) ratios were approximately
261 0.56±0.19 when the [NH_3] ranged from 0.3 μg m^{-3} to 1.8 μg m^{-3}, indicating that the
262 [$DMAH^{+*}$] and [DMA] were comparable at these [NH_3] values. Moreover, the
263 [$DMAH^{+*}$]/[NH_4^+] ratio was approximately (5±6) ×10^{-4} and DMA/NH_3 molar ratio was
264 approximately (1.8±1.0) ×10^{-3} when the [NH_3] was > 1.8 μg m^{-3}, the [$DMAH^{+}$*]/[NH_4^+]
265 ratio was (1.9±2.2) ×10^{-2} and DMA/NH_3 molar ratio was approximately (7.6±3.6) ×10^{-3}
266 when the [NH_3] was between 0.3 μg m^{-3} and 1.8 μg m^{-3}, the [$DMAH^{+}$*]/[NH_4^+] ratio
267 was 0.11±0.13 and DMA/NH_3 molar ratio was approximately (1.3±0.6) ×10^{-2} when the
268 [NH_3] < 0.3 μg m^{-3}. Combining the results suggested that the competitive uptake
269 between DMA and NH_3 on acidic aerosols appeared to be sensitive to the DMA/NH_3
270 molar ratio between 10^{-2} and 10^{-3}. Relative to NH_3, DMA may have appreciably
271 contributed to acid neutralization in $PM_{2.5}$ when the [NH_3] < 0.3 μg m^{-3}. However, it
272 was not case when the [NH_3] ≥ 0.3 μg m^{-3}.
273

274 However, not all data throughout the study, such as the circled data points in Fig 3ab,
275 followed this general trend. Higher [$DMAH^{+*}$] values and $DMAH^{+}$*/($DMAH^{+}$*+DMA)
276 ratios can be observed in the five circled cases during Period 1 (Fig 3a), when the high
277 [NH_3] values were measured. In those cases, both [$DMAH^{+*}$] and [NH_4^+] as well as SO_2
278 (9.4±4.4 μg m^{-3}) were high. In plumes rich in SO_2 and other potential acidic gases such
279 as HNO_3 (Fig S1b), the NH_3 in the marine atmosphere was likely insufficient to
280 neutralize the acids, leaving the excess acids to be neutralized by DMA. This may
281 explain the cases circled in Fig 3a during Period 2.
282
283 In addition, the calculated aerosol in-situ pH varied between 1.1 and 4.5 throughout the
284 study (Fig S1d). However, no increases in the [$DMAH^{+*}$] and
285 $DMAH^{+*}$/($DMAH^{+*}$+DMA) were observed with decreasing pH values. For example,
286 most of higher [$DMAH^{+*}$] and $DMAH^{+*}$/($DMAH^{+*}$+DMA) during Period 2-B were
287 unexpectedly associated with higher aerosol in-situ pH values (Fig 2e and S1d). The
288 same was generally true when the data between Period 2-B and Period 2-A were
289 compared.
290
291 Same with the correlations between $DMAH^{+*}$ and NH_3, the [$TMAH^{+*}$] and
292 $TMAH^{+*}$/($TMAH^{+*}$+TMA) ratio decreased with increasing [NH_3] (Fig 3c and the
293 image superimposed there). The ratio of the effective Henry's constants of TMA to NH_3
294 was estimated to be 2.6 by the E-AIM (Fig 3d, the slope of regression equation =
295 ([$TMAH^+$]/[NH_4^+]/(TMA)/[NH_3]) = ([$TMAH^+$]/[TMA]) /([NH_4^+]/[NH_3]). This ratio

was too low to compensate for the disparities between the [TMA] and [NH_3] during Period 1, leading to lower or even undetectable [$TMAH^{+*}$] at high [NH_3] values. In addition, the molar ratio of $TMAH^{+}$* to NH_4^+ in $PM_{2.5}$ was only (8.6±18) $\times10^{-3}$ during Period 2-A and (5.5±7.5) $\times10^{-3}$ during Period 2-B (Fig 2f). Thus, relative to NH_3, the TMA likely yielded a negligible contribution to acid neutralization in $PM_{2.5}$ during Period 2. The same was true during Period 1, as even smaller molar ratios were recorded.

3.4 Comparison between modeled and measured aminium concentrations

The E-AIM model was further used to examine the gas-aerosol partitioning of the species. Using the data from the entire study period, the modeled equilibrated [$DMAH^{+*}$] can be classified into three categories (Fig 4ab), as follows.

Category 1: The competitive uptake of DMA against NH_3 on acidic aerosols generally followed thermodynamic equilibria. The modeled [$DMAH^{+*}$] generally agreed with the measured values along the 1:1 line in Fig 4a. Note that this only happened when the measured [$DMAH^{+*}$] > 0.02 μg m^{-3}, which included most of data observed during Period 2-B and the periods when $DMAH^{+*}$ co-existed with NH_4^+ spikes during Period 1. In those cases, the measured [DMA] were only approximately 10% of the corresponding [$DMAH^{+*}$] in $PM_{2.5}$.

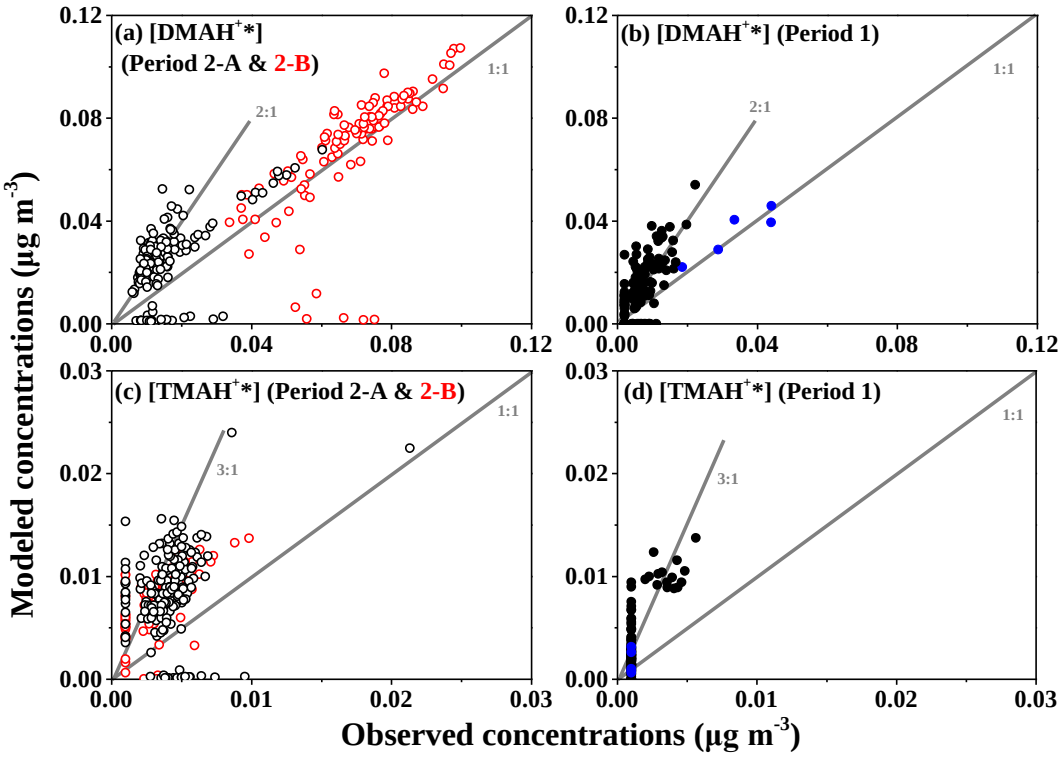

Fig 4. Modeled concentrations vs observed concentrations during different periods (Blue filled markers represent episodic $DMAH^+$, as well as $TMAH^+$, co-existing with NH_4^+ spikes during Period 1, as shown in Fig 2d and circled in Fig 3a; red empty markers represent observations during Period 2-B).

Category 2: The modeled [$DMAH^{+*}$] was generally twice that of the measured values (Fig 4ab). These cases include most of the data during Period 1 and approximately half of the data during Period 2-A. Several factors may cause these differences. First, the gas-aerosol equilibria may not have been achieved.[42] However, the estimated timescale ranged from seconds to minutes for partitioning the high volatility organic compounds into liquid particles.[43] This short equilibration timescale implies that the gas-aerosol equilibria were achieved. Additionally, a potential positive sampling artifact of DMA could have occurred on the denuder; our previous sampling analysis of NH_3 didn't observe any positive sampling artifact.[33] However, $(DMAH)_3H(SO_4)_2$ aerosol droplets have been reported to exist in NH_3–poor marine atmospheres instead of $(DMAH)_2SO_4$,

because the completely neutralized $(DMAH)_2SO_4$ solution in aerosols can convert to a $(DMAH)_3H(SO_4)_2$ solution with a molar ratio of 3:2 at a low RH in NH_3-free air[20,23]. When NH_3 and DMA gases were removed by the denuder in sampling, the conversion could cause more DMA evaporation from $PM_{2.5}$ consequently with a positive sampling of DMA gas. This needs to be verified in the future. Finally, including the scheme in laboratory observations, as reported by Chan and Chan[20] and Chu and Chan[23], might theoretically reduce the overprediction of the $[DMAH^{+*}]$ to some extent. However, the scheme was not included in the E-AIM. Overall, more experimental data are needed to fully explain the large disagreement between the modeled and measured $[DMAH^{+*}]$.

Category 3: In approximately 10% of cases, the modeled $[DMAH^{+*}]$ showed a large and negative deviation from the 1:1 line, including several data points of almost zero calculated $[DMAH^{+*}]$. This deviation also occurred for the modelled $[TMAH^{+*}]$ in the same cases. The parameter-based thermodynamics in the E-AIM does not favor $DMAH^{+*}$ and $TMAH^{+*}$ in $PM_{2.5}$ for such cases, where the calculated liquid water content was very low due to low ambient RH and/or low concentrations of ammonium salts (not shown). Considering that the $[NH_3]$ was approximately two orders of magnitude higher than the [DMA] in the marine atmosphere, $(DMAH)_3H(SO_4)_2$ aerosol particles, if they existed externally with other bisulfate aerosols, should have completely converted to ammonium sulfate, according to the thermodynamic parameters used in the E-AIM. The same can be said for TMAH-H-SO_4 particles. Thus, the modeled equilibrated $[DMAH^{+*}]$ and $[TMAH^{+*}]$ thereby approached zero and

353 ($DMAH^{+*}$+DMA) and ($TMAH^{+*}$+TMA) were overwhelmingly predicted in the gas
354 phase (Fig S2ab). Again, the reported laboratory results didn't support the complete
355 replacement of $DMAH^+$ by NH_3.[23]
356
357 The modeled [$TMAH^+$*] was generally three times that of the measured values, except
358 in cases where the equilibrated [$TMAH^{+*}$] approached zero (Fig 4c). TMAH-H-SO_4
359 aerosol droplets may exist in NH_3–poor marine atmospheres instead of $(TMAH)_2SO_4$,
360 which can convert to TMAH-H-SO_4 solution, with a molar ratio of 1:1, in NH_3-free air
361 at low RH[20,23]. For the equilibrated [$TMAH^+$*], a large positive deviation might be
362 caused by the same mechanism that explains the modeled equilibrated [$DMAH^+$*]
363 positively deviating from the observations. Moreover, in Table 2 of Chan and Chan [20],
364 the displacement of TMA sulfate by gas phase NH_3 at 50% RH is shown to be >95%.
365 Hence TMA sulfate droplets are not stable in the presence of ammonia with a significant
366 amount of TMA evaporation at 50% RH. These results suggest the possibility of
367 $TMAH^{+*}$ was displaced by NH_3, under environment of high NH_3, which was also
368 confirmed by Figure 2d and 2f, in which [$TMAH^{+*}$] shows the opposite trend with
369 [NH_4^+]. Sauerwein and Chan [18] studied the co-uptake of DMA and NH_3 by sulfuric acid
370 droplets. They found that the final $DMAH^{+*}/NH_4^+$ could be four times higher than the
371 corresponding gas phase ratio. Chan and Chan [20] also studied the evaporation of
372 aminium sulfate droplets in air. Particulate TMA sulfate yields a final composition of
373 TMA:sulfate ratio of 1:1 while particulate DMA sulfate yields DMA:sulfate ratio of
374 1.5:1 at 3%RH. Together with the fact that TMA is more volatile than DMA, these

results suggest that TMA can be easier to be displaced by NH_3 than DMA, and may contribute to the differences between the observed trends of $DMAH^{+*}$ and $TMAH^{+*}$ in this study. However, those laboratory experiments were conducted at virtually TMA free atmosphere. More detailed experiments mimicking the ambient conditions will need to be conducted for confirmation. The large negative deviation in approximately 10% of the cases was likely caused by the same mechanism that explains the modeled equilibrated [$DMAH^{+}$*] in the same cases.

Overall, the predicted gas-aerosol equilibria were able to explain the observed high [$DMAH^{+*}$] values during Period 2-B. However, the observation that the [$TMAH^{+*}$] was an order of magnitude lower than the [$DMAH^{+*}$], although their gaseous counterparts had comparable concentrations, in this case, the predicted gas-aerosol equilibria cannot be explained because the E-AIM model predicted approximately three times the observed [$TMAH^{+*}$].

3.5 Period 2B: *Decreased [$TMAH^{+*}$] and increased [$DMAH^{+}$*] in the presence of [NH_4^+] spikes*

During the [NH_4^+] spikes, the [$DMAH^{+*}$] and $DMAH^{+*}$/($DMAH^{+*}$+DMA) ratio increased, but the [$TMAH^{+*}$] and $TMAH^{+*}$/($TMAH^{+*}$+TMA) ratio decreased. We focused on Period 2-B (Fig 5a-d; zoom in on Period 2-B to allow the detailed spatiotemporal variations of particulate ions and SO_2 to be clearly identified), when the [$DMAH^{+*}$] and [NH_4^+] were positively correlated ($P<0.01$) and the [$TMAH^{+*}$] and

397 [NH_4^+] ($P<0.01$) were negatively correlated (Fig 5e). As mentioned above, the presence
398 of excess acids may increase both the [$DMAH^{+*}$] and [NH_4^+] at low [NH_3] values. In
399 addition, the modeled aerosol pH was approximately 2.3±0.9, with a maximum value
400 of 4.5, during this period (Fig 5d), which is consistent with the values reported in NH_3-
401 poor coastal and marine atmospheres[44-46] and favors DMA partitioning in $PM_{2.5}$ at low
402 [NH_3] values, as predicted by the E-AIM.
403
404 During the blue highlighted [$TMAH^{+*}$] trough in Period 2-B, the pH values were
405 3.1±0.8, which was approximately seven units smaller than the pK_a of the $TMAH^+$ [1].
406 Under such acidic conditions, TMA should behave similarly to DMA and
407 predominantly exist in the particle phase; however, this study observed a decrease in
408 the [$TMAH^+$*] with an increasing [NH_4^+] in the plume containing excess acids.
409
410 These results suggest the possibility of $TMAH^{+*}$ was displaced by NH_3, under
411 environment of high NH_3, which was also supported by Figure 2d and 2f, in which
412 [$TMAH^{+*}$] shows the opposite trend with [NH_4^+], which was discussed in the previous
413 section.
414
415 Supposed that the gas-aerosol equilibria had been achieved and no other chemical
416 reactions occurred besides neutralization, the [$TMAH^{+*}$+TMA] should be invariant
417 with decreasing [$TMAH^{+*}$] in $PM_{2.5}$. However, the [$TMAH^{+*}$+TMA] decreased with a
418 decreasing [$TMAH^{+*}$] during Period 2-B (Fig 5f). In addition, no increase in the [TMA]

occurred with a decreasing [$TMAH^{+*}$] (image superimposed in Fig 5f). Any additional TMA in the system should have partitioned to the particle phase. Recently, Berndt et al. reported that TMA can form highly oxidized products via the most efficient atmospheric autoxidation currently known.[47] OH radicals are formed from photochemical processes in both gas phase transfer and in-situ aqueous phase,[48] some photochemical processes such as nitrate or nitrite photolysis[49,50], hydrogen peroxide (H_2O_2) photolysis, and photo-Fenton processes[48] are important sources of OH radicals. Highly formed OH radicals in the atmosphere may trigger the efficient oxidation of the three methyl groups of TMA.[47] Unfortunately, highly oxidized organic nitrogen products cannot be detected by the AIM-IC. Overall, the decrease in the [$TMAH^{+*}$] during [NH_4^+] spikes suggests that the chemical conversion of $TMAH^{+*}$ to other nitrogen compounds must be considered to fully understand the behaviors of TMA species in marine atmospheres, in addition to acid-base neutralization reactions.

In summary, the [NH_3] varied by over one order of magnitude during the cruise and led to the DMA/NH_3 and TMA/NH_3 molar ratios varying from 10^{-3} to 10^{-2}. The competitive uptake of DMA and TMA against NH_3 on acidic aerosols largely reduced when the amine to ammonia ratio decreased from 10^{-2} to 10^{-3} mainly because of increased [NH_3]. However, in the presence of excess acids, the [$DMAH^+$] increased with the [NH_4^+], even at high [NH_3] values. The uptake of TMA is still not fully understood; for example, the E-AIM predicted that the [$TMAH^+$] should be approximately three times that of the observations in the presence of abundant NH_4^+.

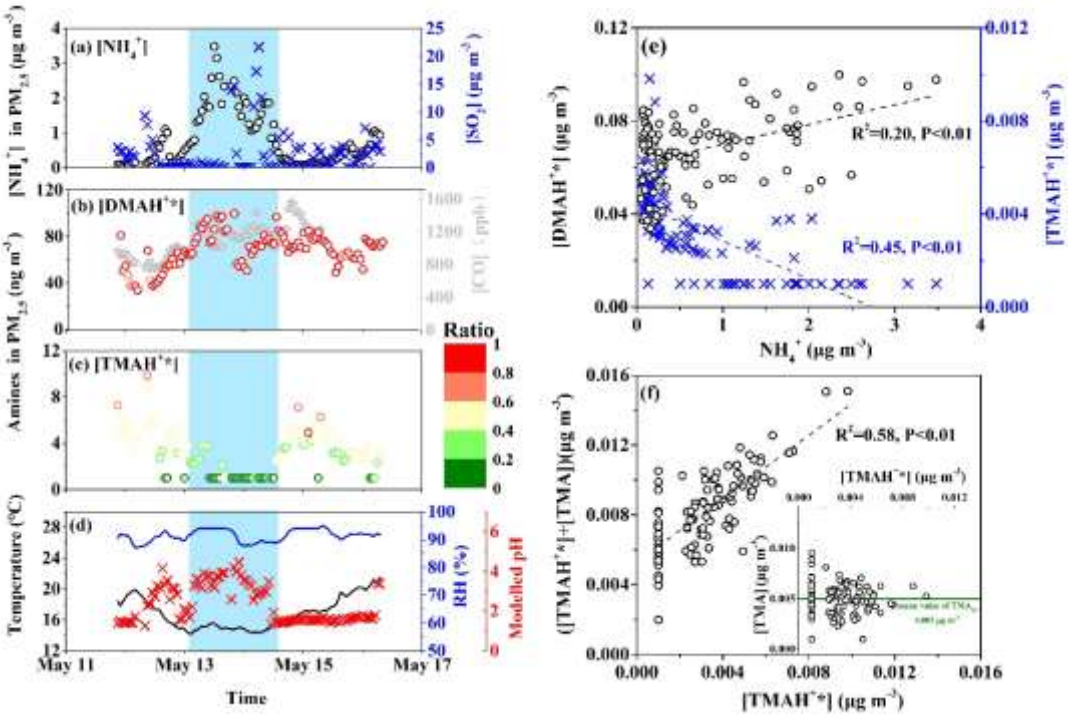

Fig 5. Time series of the concentrations of particulate ions, SO_2, CO, ambient conditions, and modeled pH, as well as correlation analysis of the variables during Period 2-B. (a) particulate NH_4^+ and SO_2; (b) particulate $DMAH^{+*}$ and CO; (c) particulate $TMAH^{+*}$; (d) ambient temperature, RH, and modelled pH; (e) $DMAH^{+}$* and $TMAH^{+}$* vs. NH_4^+ in $PM_{2.5}$; (f) ($TMAH^{+*}$+TMA) vs $TMAH^{+}$* in $PM_{2.5}$. The colored bars represent the ratios of $DMAH^{+*}$/($DMAH^{+*}$+DMA) in (b) and $TMAH^{+*}$/($TMAH^{+*}$+TMA) in (c); the trough in $TMAH^+$ is highlighted in light blue.

Supporting Information

Text S1. Detection limits for ions during the cruise study
Table S1. The detection limits for NH_4^+, $DMAH^+$, $TMAH^+$, NO_3^- and SO_4^{2-}
Table S2. The comparison of DL/2 substitution and Kaplan – Meier (KM) procedure to process the ratios of data that include nondetects(NDs).
Figure S1. Time series of the gas and particulate ion concentrations, as well as ambient conditions and modeled pH during the whole cruise.
Figure S2. Modeled [DMA] and [TMA] versus the observations in Period 2-B.

Acknowledgement

This research is supported by the Natural Science Foundation of China (grant no.

41776086), the National Key Research and Development Program in China (grant no. 2016YFC0200504), the Natural Science Foundation of China (grant no. 41875142, 41905122, 42075100), and the Hong Kong Research Grants Council (grant no. 11302318).

References

(1) Ge, X.; Wexler, A. S.; Clegg, S. L. Atmospheric amines -Part II. Thermodynamic properties and gas/particle partitioning. Atmos. Environ. 2011, 45 (3), 561–577. DOI: 10.1016/j.atmosenv.2010.10.013.

(2) Zheng, J.; Ma, Y.; Chen, M.; Zhang, Q.; Wang, L.; Khalizov, A. F.; Yao, L.; Wang, Z.; Wang, X.; Chen, L. Measurement of atmospheric amines and ammonia using the high resolution time-of-flight chemical ionization mass spectrometry. Atmos. Environ. 2015, 102, 249–259. DOI: 10.1016/j.atmosenv.2014.12.002.

(3) Kürten, A.; Bergen, A.; Heinritzi, M.; Leiminger, M.; Lorenz, V.; Piel, F.; Simon, M.; Sitals, R.; Wagner, A. C.; Curtius, J. Observation of new particle formation and measurement of sulfuric acid, ammonia, amines and highly oxidized organic molecules at a rural site in central Germany. Atmos. Chem. Phys. 2016, 16 (19), 12793–12813. DOI: 10.5194/acp-16-12793-2016.

(4) Almeida, J.; Schobesberger, S.; Kürten, A.; Ortega, I. K.; Kupiainen-Määttä, O.; Praplan, A. P.; Adamov, A.; Amorim, A.; Bianchi, F.; Breitenlechner, M.; David, A.; Dommen, J.; Donahue, N. M.; Downard, A.; Dunne, E.; Duplissy, J.; Ehrhart, S.; Flagan, R. C.; Franchin, A.; Guida, R.; Hakala, J.; Hansel, A.; Heinritzi, M.; Henschel, H.; Jokinen, T.; Junninen, H.; Kajos, M.; Kangasluoma, J.; Keskinen, H.; Kupc, A.; Kurtén, T.; Kvashin, A. N.; Laaksonen, A.; Lehtipalo, K.; Leiminger, M.; Leppä, J.; Loukonen, V.; Makhmutov, V.; Mathot, S.; McGrath, M. J.; Nieminen, T.; Olenius, T.; Onnela, A.; Petäjä, T.; Riccobono, F.; Riipinen, I.; Rissanen, M.; Rondo, L.; Ruuskanen, T.; Santos, F. D.; Sarnela, N.; Schallhart, S.; Schnitzhofer, R.; Seinfeld, J. H.; Simon, M.; Sipilä, M.; Stozhkov, Y.; Stratmann, F.; Tomé, A.; Tröstl, J.; Tsagkogeorgas, G.; Vaattovaara, P.; Viisanen, Y.; Virtanen, A.; Vrtala, A.; Wagner, P. E.; Weingartner, E.; Wex, H.;

Williamson, C.; Wimmer, D.; Ye, P.; Yli-Juuti, T.; Carslaw, K. S.; Kulmala, M.; Curtius, J.; Baltensperger, U.; Worsnop, D. R.; Vehkamäki, H.; Kirkby, J. Molecular understanding of sulphuric acid-amine particle nucleation in the atmosphere. Nature 2013, 502 (7471), 359–363. DOI: 10.1038/nature12663.

(5) Chen, H.; Varner, M. E.; Gerber, R. B.; Finlayson-Pitts, B. J. Reactions of Methanesulfonic Acid with Amines and Ammonia as a Source of New Particles in Air. J. Phy. Chem. B 2016, 120 (8), 1526–1536. DOI: 10.1021/acs.jpcb.5b07433.

(6) Tao, Y.; Ye, X.; Jiang, S.; Yang, X.; Chen, J.; Xie, Y.; Wang, R. Effects of amines on particle growth observed in new particle formation events. J. Geophys. Res. Atmos. 2016, 121 (1), 324–335. DOI: 10.1002/2015JD024245.

(7) Yao, L.; Garmash, O.; Bianchi, F.; Zheng, J.; Yan, C.; Kontkanen, J.; Junninen, H.; Mazon, S. B.; Ehn, M.; Paasonen, P.; Sipilä, M.; Wang, M.; Wang, X.; Xiao, S.; Chen, H.; Lu, Y.; Zhang, B.; Wang, D.; Fu, Q.; Geng, F.; Li, L.; Wang, H.; Qiao, L.; Yang, X.; Chen, J.; Kerminen, V.-M.; Petäjä, T.; Worsnop, D. R.; Kulmala, M.; Wang, L. Atmospheric new particle formation from sulfuric acid and amines in a Chinese megacity. Science 2018, 361 (6399), 278–281. DOI: 10.1126/science.aao4839.

(8) Chan, C. K.; Yao, X. Air pollution in mega cities in China. Atmospheric Environment 2008, 42 (1), 1–42. DOI: 10.1016/j.atmosenv.2007.09.003.

(9) Seinfeld, J. H.; Pandis, S. N., Eds. Atmospheric Chemistry and Physics: From Air Pollution to Climate Change, John Wiley & Sons, Inc, 1997, 523-539.

(10) Carpenter, L. J.; Archer, S. D.; Beale, R. Ocean-atmosphere trace gas exchange. Chem. Soc. Rev. 2012, 41 (19), 6473–6506. DOI: 10.1039/c2cs35121h.

(11) Behera, S. N.; Sharma, M.; Aneja, V. P.; Balasubramanian, R. Ammonia in the atmosphere: a review on emission sources, atmospheric chemistry and deposition on terrestrial bodies. Environ. Sci. Pollut. Res. Int. 2013, 20 (11), 8092–8131. DOI: 10.1007/s11356-013-2051-9.

(12) Paulot, F.; Jacob, D. J.; Pinder, R. W.; Bash, J. O.; Travis, K.; Henze, D. K. Ammonia emissions in the United States, European Union, and China derived by high-resolution inversion of ammonium wet deposition data: Interpretation with a new agricultural emissions inventory (MASAGE_NH3). J. Geophys. Res. Atmos. 2014, 119

(7), 4343–4364. DOI: 10.1002/2013JD021130.

(13) Schiferl, L. D.; Heald, C. L.; Nowak, J. B.; Holloway, J. S.; Neuman, J. A.; Bahreini, R.; Pollack, I. B.; Ryerson, T. B.; Wiedinmyer, C.; Murphy, J. G. An investigation of ammonia and inorganic particulate matter in California during the CalNex campaign. J. Geophys. Res. Atmos. 2014, 119 (4), 1883–1902. DOI: 10.1002/2013JD020765.

(14) Tang, Y. S.; Braban, C. F.; Dragosits, U.; Dore, A. J.; Simmons, I.; van Dijk, N.; Poskitt, J.; Dos Santos Pereira, G.; Keenan, P. O.; Conolly, C.; Vincent, K.; Smith, R. I.; Heal, M. R.; Sutton, M. A. Drivers for spatial, temporal and long-term trends in atmospheric ammonia and ammonium in the UK. Atmos. Chem. Phys. 2018, 18 (2), 705–733. DOI: 10.5194/acp-18-705-2018.

(15) Liu, L.; Zhang, X.; Wong, A. Y. H.; Xu, W.; Liu, X.; Li, Y.; Mi, H.; Lu, X.; Zhao, L.; Wang, Z.; Wu, X.; Wei, J. Estimating global surface ammonia concentrations inferred from satellite retrievals. Atmos. Chem. Phys. 2019, 19 (18), 12051–12066. DOI: 10.5194/acp-19-12051-2019.

(16) Xie, H.; Feng, L.; Hu, Q.; Zhu, Y.; Gao, H.; Gao, Y.; Yao, X. Concentration and size distribution of water-extracted dimethylaminium and trimethylaminium in atmospheric particles during nine campaigns - Implications for sources, phase states and formation pathways. Sci. Total Environ. 2018, 631-632, 130–141. DOI: 10.1016/j.scitotenv.2018.02.303.

(17) Hu, Q.; Qu, K.; Gao, H.; Cui, Z.; Gao, Y.; Yao, X. Large Increases in Primary Trimethylaminium and Secondary Dimethylaminium in Atmospheric Particles Associated With Cyclonic Eddies in the Northwest Pacific Ocean. J. Geophys. Res. Atmos. 2018, 123 (21), 12,133-12,146. DOI: 10.1029/2018JD028836.

(18) Sauerwein, M.; Chan, C. K. Heterogeneous uptake of ammonia and dimethylamine into sulfuric and oxalic acid particles. Atmos. Chem. Phys. 2017, 17 (10), 6323–6339. DOI: 10.5194/acp-17-6323-2017.

(19) Youn, J.-S.; Crosbie, E.; Maudlin, L. C.; Wang, Z.; Sorooshian, A. Dimethylamine as a major alkyl amine species in particles and cloud water: Observations in semi-arid and coastal regions. Atmos. Environ. 2015, 122, 250–258. DOI:

10.1016/j.atmosenv.2015.09.061.

(20) Chan, L. P.; Chan, C. K. Role of the aerosol phase state in ammonia/amines exchange reactions. Environ. Sci. Technol. 2013, 47 (11), 5755–5762. DOI: 10.1021/es4004685.

(21) Qiu, C.; Zhang, R. Multiphase chemistry of atmospheric amines. Phys. Chem. Chem. Phys. 2013, 15 (16), 5738–5752. DOI: 10.1039/c3cp43446j.

(22) DeRieux, W.-S. W.; Lakey, P. S. J.; Chu, Y.; Chan, C. K.; Glicker, H. S.; Smith, J. N.; Zuend, A.; Shiraiwa, M. Effects of Phase State and Phase Separation on Dimethylamine Uptake of Ammonium Sulfate and Ammonium Sulfate–Sucrose Mixed Particles. ACS Earth Space Chem. 2019, 3 (7), 1268–1278. DOI: 10.1021/acsearthspacechem.9b00142.

(23) Chu, Y.; Chan, C. K. Reactive Uptake of Dimethylamine by Ammonium Sulfate and Ammonium Sulfate-Sucrose Mixed Particles. J. Phys. Chem. A 2017, 121 (1), 206–215. DOI: 10.1021/acs.jpca.6b10692.

(24) Pankow, J. F. Phase considerations in the gas/particle partitioning of organic amines in the atmosphere. Atmos. Environ. 2015, 122, 448–453. DOI: 10.1016/j.atmosenv.2015.09.056.

(25) Wang, L.; Khalizov, A. F.; Zheng, J.; Xu, W.; Ma, Y.; Lal, V.; Zhang, R. Atmospheric nanoparticles formed from heterogeneous reactions of organics. Nature Geoscience 2010, 3 (4), 238–242. DOI: 10.1038/ngeo778.

(26) Yu, F.; Luo, G. Modeling of gaseous methylamines in the global atmosphere: impacts of oxidation and aerosol uptake. Atmos. Chem. Phys. 2014, 14 (22), 12455–12464. DOI: 10.5194/acp-14-12455-2014.

(27) Bergman, T.; Laaksonen, A.; Korhonen, H.; Malila, J.; Dunne, E. M.; Mielonen, T.; Lehtinen, K. E. J.; Kühn, T.; Arola, A.; Kokkola, H. Geographical and diurnal features of amine-enhanced boundary layer nucleation. J. Geophys. Res. Atmos. 2015, 120 (18), 9606–9624. DOI: 10.1002/2015JD023181.

(28) Mao, J.; Yu, F.; Zhang, Y.; An, J.; Wang, L.; Zheng, J.; Yao, L.; Luo, G.; Ma, W.; Yu, Q.; Huang, C.; Li, L.; Chen, L. High-resolution modeling of gaseous methylamines over a polluted region in China: source-dependent emissions and implications of spatial

580 variations. Atmos. Chem. Phys. 2018, 18 (11), 7933–7950. DOI: 10.5194/acp-18-7933-
581 2018.
582 (29) VandenBoer, T. C.; Petroff, A.; Markovic, M. Z.; Murphy, J. G. Size distribution
583 of alkyl amines in continental particulate matter and their online detection in the gas
584 and particle phase. Atmos. Chem. Phys. 2011, 11 (9), 4319–4332.
585 (30) You, Y.; Kanawade, V. P.; Gouw, J. A. de; Guenther, A. B.; Madronich, S.; Sierra-
586 Hernández, M. R.; Lawler, M.; Smith, J. N.; Takahama, S.; Ruggeri, G.; Koss, A.; Olson,
587 K.; Baumann, K.; Weber, R. J.; Nenes, A.; Guo, H.; Edgerton, E. S.; Porcelli, L.; Brune,
588 W. H.; Goldstein, A. H.; Lee, S.-H. Atmospheric amines and ammonia measured with
589 a chemical ionization mass spectrometer (CIMS). Atmos. Chem. Phys. 2014, 14 (22),
590 12181–12194. DOI: 10.5194/acp-14-12181-2014.
591 (31) Yao, L.; Wang, M.-Y.; Wang, X.-K.; Liu, Y.-J.; Chen, H.-F.; Zheng, J.; Nie, W.;
592 Ding, A.-J.; Geng, F.-H.; Wang, D.-F.; Chen, J.-M.; Worsnop, D. R.; Wang, L. Detection
593 of atmospheric gaseous amines and amides by a high-resolution time-of-flight chemical
594 ionization mass spectrometer with protonated ethanol reagent ions. Atmos. Chem. Phys.
595 2016, 16 (22), 14527–14543. DOI: 10.5194/acp-16-14527-2016.
596 (32) Shi, J.-H.; Zhang, J.; Gao, H.-W.; Tan, S.-C.; Yao, X.-H.; Ren, J.-L. Concentration,
597 solubility and deposition flux of atmospheric particulate nutrients over the Yellow Sea.
598 Deep-Sea Res. 2013, 97, 43–50. DOI: 10.1016/j.dsr2.2013.05.004.
599 (33) Helsel, D. R.. Summing nondetects: Incorporating low-level contaminants in
600 risk assessment. Integr. Environ. Asses. 2010, 6(3), 361-366.DOI: 10.1002/ieam.31
601 (34) Teng, X.; Hu, Q.; Zhang, L.; Qi, J.; Shi, J.; Xie, H.; Gao, H.; Yao, X. Identification
602 of Major Sources of Atmospheric NH_3 in an Urban Environment in Northern China
603 During Wintertime. Environ. Sci. Technol. 2017, 51 (12), 6839–6848. DOI:
604 10.1021/acs.est.7b00328.
605 (35) Clegg, S. L.; Qiu, C.; Zhang, R. The deliquescence behaviour, solubilities, and
606 densities of aqueous solutions of five methyl- and ethyl-aminium sulphate salts. Atmos.
607 Environ. 2013, 73, 145–158. DOI: 10.1016/j.atmosenv.2013.02.036.
608 (36) Shiraiwa, M.; Li, Y.; Tsimpidi, A.; Karydis, V.; Berkemeier, T.; Pandis, S.;
609 Lelieveld, J.; Koop, T.; Pöschl, U. Global distribution of particle phase state in

610 atmospheric secondary organic aerosols. Nat. Commun. 2017, 8, 15002. DOI:
611 10.1038/ncomms15002.
612 (37) Quinn, P. K.; Collins, D. B.; Grassian, V. H.; Prather, K. A.; Bates, T. S. Chemistry
613 and related properties of freshly emitted sea spray aerosol. Chem. Rev. 2015, 115 (10),
614 4383–4399. DOI: 10.1021/cr500713g.
615 (38) Prather, K. A.; Bertram, T. H.; Grassian, V. H.; Deane, G. B.; Stokes, M. D.;
616 Demott, P. J.; Aluwihare, L. I.; Palenik, B. P.; Azam, F.; Seinfeld, J. H.; Moffet, R. C.;
617 Molina, M. J.; Cappa, C. D.; Geiger, F. M.; Roberts, G. C.; Russell, L. M.; Ault, A. P.;
618 Baltrusaitis, J.; Collins, D. B.; Corrigan, C. E.; Cuadra-Rodriguez, L. A.; Ebben, C. J.;
619 Forestieri, S. D.; Guasco, T. L.; Hersey, S. P.; Kim, M. J.; Lambert, W. F.; Modini, R.
620 L.; Mui, W.; Pedler, B. E.; Ruppel, M. J.; Ryder, O. S.; Schoepp, N. G.; Sullivan, R. C.;
621 Zhao, D. Bringing the ocean into the laboratory to probe the chemical complexity of
622 sea spray aerosol. PNAS 2013, 110 (19), 7550–7555. DOI: 10.1073/pnas.1300262110.
623 (39) Yu, P.; Hu, Q.; Li, K.; Zhu, Y.; Liu, X.; Gao, H.; and Yao, X. Characteristics of
624 dimethylaminium and trimethylaminium in atmospheric particles ranging from
625 supermicron to nanometer sizes over eutrophic marginal seas of China and oligotrophic
626 open oceans. Sci. Total Environ. 2016, 572, 813–824.
627 DOI:10.1016/j.scitotenv.2016.07.114.
628 (40) Hu, Q.; Yu, P.; Zhu, Y.; Li, K.; Gao, H.; and Yao, X. Concentration, size
629 distribution, and formation of trimethylaminium and dimethylaminium ions in
630 atmospheric particles over marginal seas of China. J. Atmos. Sci. 2015, 72(9), 3487–
631 3498. DOI:10.1175/JAS-D-14-0393.1.
632 (41) Chen, D., Shen, Y., Wang, J., Gao, Y., Gao, H., Yao, X. Mapping gaseous
633 dimethylamine, trimethylamine, ammonia, and their particulate counterparts in marine
634 atmospheres of China's marginal seas – Part 1: Differentiating marine emission from
635 continental transport. Atmos. Chem. Phys. 2021, 21(21), 16413–16425. DOI:
636 10.5194/acp-21-16413-2021.
637 (42) Wexler, A. S.; Seinfeld, J.H. The distribution of ammonium salts among a size and
638 composition dispersed aerosol. Atmos. Environ. 1990. 24(5), 1231-1246.
639 DOI:10.1016/0960-1686(90)90088-5

(43) Shiraiwa, M.; Seinfeld, J.H. Equilibration timescale of atmospheric secondary organic aerosol partitioning. Geophys. Res. Lett. 2012, 39(24), L24801, DOI: 10.1029/2012GL054008.

(44) Yao, X.; Yan Ling, Tsz.; Fang, M.; Chan, Chak K. Comparison of thermodynamic predictions for in situ pH in $PM_{2.5}$. Atmos. Environ. 2006, 40(16), 2835-2844. DOI: 10.1016/j.atmosenv.2006.01.006.

(45) Yao, X.; Yan Ling, Tsz.; Fang, M.; Chan, Chak K. Size dependence of in situ pH in submicron atmospheric particles in Hong Kong. Atmos. Environ. 2007, 41(2), 382-393. DOI:10.1016/j.atmosenv.2006.07.037

(46) Pye H. O. T.; Nenes, A.; Alexander, B.; Ault, A. P.; Barth, M. C.; Clegg, S. L.; Collett Jr., J. L.; Fahey, K. M.; Hennigan, C. J.; Herrmann, H.; Kanakidou, M.; Kelly, J. T.; Ku, I.-T.; McNeill, V. F.; Riemer, N.; Schaefer, T.; Shi, G.; Tilgner, A.; Walker, J. T.; Wang, T.; Weber, R.; Xing, J.; Zaveri, R. A.; Zuend, A. The acidity of atmospheric particles and clouds. Atmos. Chem. Phys. 2020, 20(8), 4809-4888. DOI:10.5194/acp-20-4809-2020.

(47) Berndt, T.; Møller, K.H.; Herrmann, H.; Kjaergaard H.G. Trimethylamine outruns terpenes and aromatics in atmospheric autoxidation. J Phys. Chem. A, 2021. 125(20), 4454–4466. DOI: 10.1021/acs.jpca.1c02465.

(48) Li, M.; Karu, E.; Brenninkmeijer, C.; Fischer, H.; Lelieveld, J.; Williams, J. Tropospheric OH and stratospheric OH and Cl concentrations determined from CH_4, CH_3Cl, and SF_6 Measurements. Npj Clim. Atmos. Sci. 2018, 1(1), 1-7. DOI: 10.1038/s41612-018-0041-9.

(49) Gligorovski, S.; Strekowski, R.; Barbati, S.; Vione, D. Environmental implications of hydroxyl radicals (•OH). Chem. Rev. 2015, 115 (24), 13051–13092. DOI: 10.1021/cr500310b.

(50) Gen, M.; Zhang, R.; Huang, D. D.; Li, Y.; Chan, C. K. Heterogeneous SO_2 oxidation in sulfate formation by photolysis of particulate nitrate. Environ. Sci. Technol. Lett. 2019, 6 (2), 86–91. DOI: 10.1021/acs.estlett.8b00681.